Zero-Sequence Voltage Reduces DC-Link Capacitor Demand in Cascaded H-Bridge Converters for Large-Scale Electrolyzers by 40 %

Roland Unruh, Frank Schafmeister, Joachim Böcker
Paderborn University
Warburger Str. 100
Paderborn, Germany
Tel.: +49/ (05251) 60-3492
Fax.: +49/ (05251) 60-3443
E-Mail: unruh@lea.uni-paderborn.de
URL: http://lea.upb.de

Keywords

≪Cascaded H-Bridge≫, ≪Solid-State Transformer≫, ≪Zero sequence voltage≫, ≪Third harmonic injection≫, ≪Capacitor voltage balancing≫

Acknowledgments

The authors would like to thank the German Research Foundation (DFG) for the funding the research under the project number 456097802.

Abstract

Cascaded H-bridge Converters (CHBs) are a promising solution in converting power from a three-phase medium voltage of 6.6 kV...30 kV to a lower DC-voltage in the range of 100 V...1 kV to provide pure DC power to applications such as electrolyzers for hydrogen generation, data centers with a DC power distribution and DC microgrids. CHBs can be interpreted as modular multilevel converters with an isolated DC-DC output stage per module, require a large DC-link capacitor for each module to handle the second harmonic voltage ripple caused by the fluctuating input power within a fundamental grid period. Without a zero-sequence voltage injection, star-connected CHBs are operated with approximately sinusoidal arm voltages and currents. The floating star point potential enables to utilize different zero-sequence voltage injection techniques such as a third-harmonic injection with $\frac{1}{6}$ of the grid voltage amplitude or a Min-Max voltage injection. Both well-known methods have the advantage to reduce the peak arm voltage and thereby the number of required modules by 13.4 % (to $\frac{\sqrt{3}}{2}$). This paper proves analytically that the third-harmonic injection with $\frac{1}{6}$ of the grid voltage amplitude reduces the second harmonic voltage ripple by only 15.1 % compared to no-voltage injection for unity power factor operation and balanced grid voltages. Then it is shown, that the Min-Max injection has the often overlooked advantage of reducing the second harmonic voltage ripple by even 18.8 %. By applying the here proposed zero-sequence voltage injection in saturation modulation, the second harmonic voltage ripple of the DC-link capacitors is reduced by even 24.3 %, while still requiring the same number of modules as the Min-Max injection. For a realistic number of reserve modules, the overall energy ripple in the DC-link capacitors is reduced by 40 %.

I. Introduction

High-power DC loads such as industrial water electrolyzers [1–3] require high DC currents up to 5 kA in the low-voltage range of 100 V...1 kV [4, 5]. The same applies for data centers with a 400 V and 800 V DC power distribution [6, 7] as well as for ultra-fast electric vehicle charging [8]. The state of the art is a centralized line frequency medium voltage transformer to convert the three-phase medium voltage of 6.6 kV...30 kV to a low AC voltage that is rectified for the load [5, 9, 10]. The transformer has usually secondary windings in delta and star configuration to allow a 12-pulse rectifier to generate the required DC load voltage. However, a 12-pulse thyristor rectifier increases the specific energy consumption of an

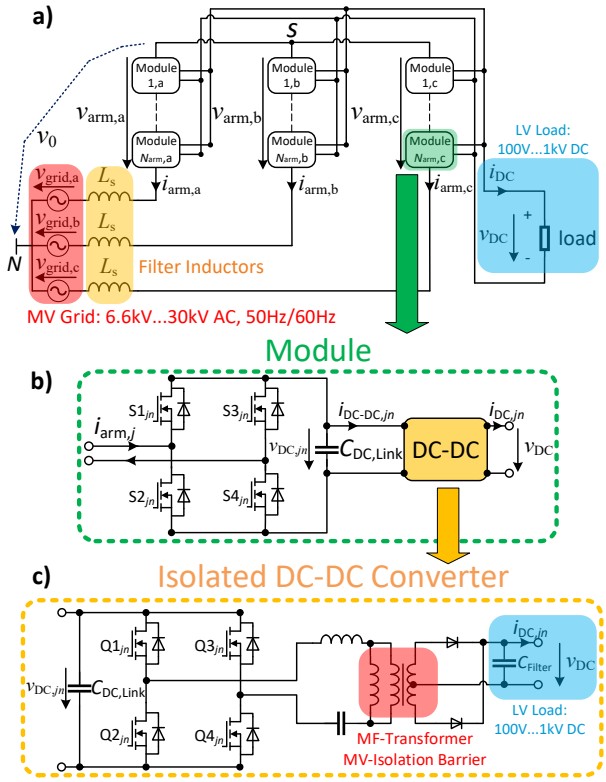

Fig. 1: The three-phase cascaded H-bridge converter a) consists of identical modules b). Each DC-DC converter c) transfers power to the load [20].

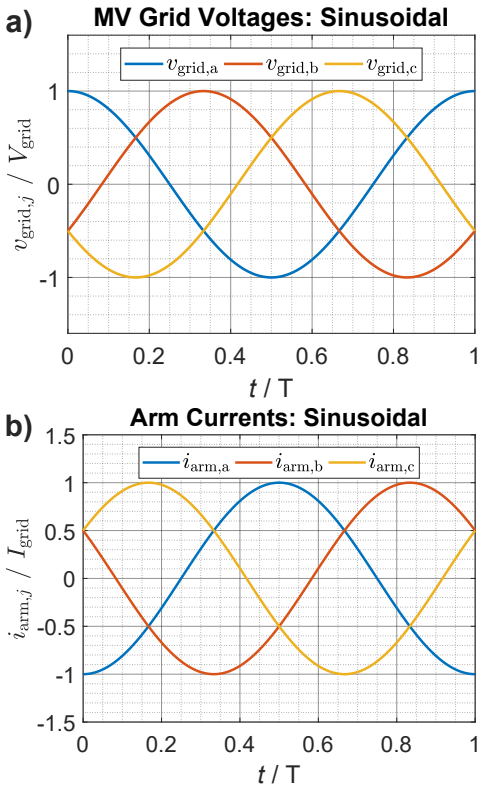

Fig. 2: The line-to-neutral grid voltages $v_{\mathrm{grid},j}$ in a) and arm currents $i_{\mathrm{arm},j}$ in b) are sinusoidal. Harmonic current injections are not allowed [14].

electrolyzer stack by around 9 % [11] due to the DC current ripple. Additionally, thyristor rectifiers show a low power factor for high firing angles at low load [12]. A 12-pulse diode rectifier [5] with subsequent buck converters improves the power factor and the specific energy consumption [11]. Still, it requires additional active and/or passive filters to achieve low grid-side current harmonics [13].
Therefore, a system is required that achieves nearly sinusoidal grid currents [14] and a controllable power factor [15–17] for inductive, capacitive and unity power factor operation. Additionally, it should not rely on a single component such as a central line- or medium-frequency transformer [18]. This can be achieved by using the three-phase cascaded H-bridge Converter (CHB) [19] with star configuration shown in Fig. 1 a). In this cascaded structure, an isolated full-bridge DC-DC converter [20] is connected to each module capacitor $C_{\mathrm{DC,Link}}$, which converts the module voltage to a lower output voltage v_{DC} shown e.g. in Fig. 1 c). The transferred power of each DC-DC converter is controlled on each module locally by adjusting the switching frequency and phase-shift [21, 22]. The bulky line-frequency transformer (LFT) is replaced by multiple smaller medium-frequency transformers (MFTs) within the DC-DC converters providing the required galvanic isolation. The low DC-voltage v_{DC} can be used directly for DC applications such as electrolysis and data center distribution buses or be converted via DC-AC converters into a three-phase voltage in order to replace a low-frequency distribution transformer [23].

For the purposes of this paper, the load will be considered as a large-scale electrolyzer with unidirectional power flow. However, the developed zero-sequence injection can be transferred to bidirectional CHBs or to large-scale photovoltaic (PV) CHBs because in both cases the power factor is $\cos(\phi) = 1$, if there is no significantly unbalanced PV generation. However, the results can not be transfered to cascaded multilevel static compensators (STATCOMs) directly because they have a power factor of $\cos(\phi) \approx 0$.
The main focus of this article, is to minimize the required capacitance of the module capacitors $C_{\mathrm{DC,Link}}$ by reducing the second harmonic voltage ripple by shifting the star points potential s in Fig. 1 a). Altering the output power of the isolated DC-DC converters is also possible [24], but it increases the losses and

is disregarded in this article. Still, the presented techniques are expected to be beneficial for open-loop operated DC-DC converters due to the reduced peak arm input power.
This paper is organized as follows: the second harmonic voltage ripple is calculated with normalized arm currents and voltages for no zero-sequence injection in Section II. In Section III, the benefits of the commonly used third-harmonic voltage injection with $\frac{1}{6}$ of the grid-voltage amplitude are briefly shown. In Section IV, it is proven numerically, that the also commonly used Min-Max voltage injection requires the same arm voltages as the third-harmonic injection, but allow to further reduce $C_{\mathrm{DC,Link}}$ by 4.4 % without increasing the second harmonic voltage ripple. Going further, a new method is presented in Section V, which usually operates one of the three arms at its voltage limit and reduces the second harmonic voltage ripple by between 24 % and 40 % without the need for additional hardware. Finally, Section VI presents the conclusion.

II. Nominal Operation: No Zero-Sequence Voltage Injection

For the purposes of the paper, the three-phase grid voltages are balanced and can be expressed as follows:

$$\begin{aligned} v_{\mathrm{grid,a}}(t) &= V_{\mathrm{grid}} \cos(\omega t) \\ v_{\mathrm{grid,b}}(t) &= V_{\mathrm{grid}} \cos(\omega t - 2\pi/3) \\ v_{\mathrm{grid,c}}(t) &= V_{\mathrm{grid}} \cos(\omega t + 2\pi/3) \end{aligned} \tag{1}$$

Ideally, the arm currents are controlled to be sinusoidal and in phase with the grid voltages [25]. The negative sign results from the fact, that power is transferred from the grid to the load. The resulting currents are expressed as:

$$\begin{aligned} i_{\mathrm{arm,a}}(t) &= -I_{\mathrm{grid}} \cos(\omega t) \\ i_{\mathrm{arm,b}}(t) &= -I_{\mathrm{grid}} \cos(\omega t - 2\pi/3) \\ i_{\mathrm{arm,c}}(t) &= -I_{\mathrm{grid}} \cos(\omega t + 2\pi/3) \end{aligned} \tag{2}$$

The grid voltages and arm currents are shown in Fig. 2. The arm voltages show a high-frequency component due to the modulation, which can be neglected for sufficiently high switching frequencies [26] and DC-link voltage balancing [27].

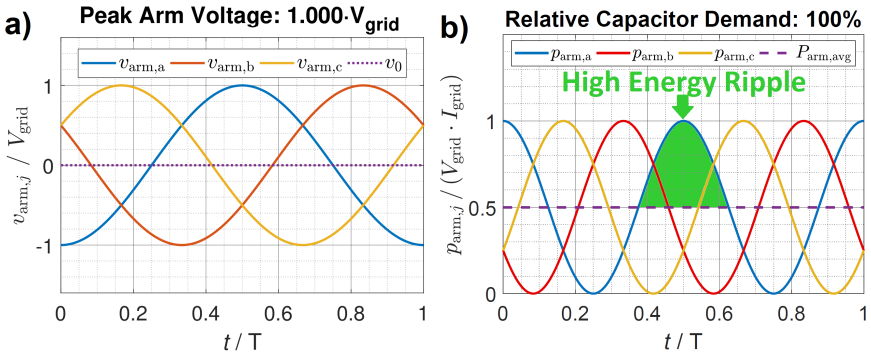

Fig. 3: Resulting arm voltages a) and input power b) for no zero-sequence voltage injection. The required arm voltage and DC-link capacitance are high and normalized to 100 %.

Furthermore, the voltage drop across the filter inductors L_{s} is approximately 1 % of the grid voltage. Therefore, the filter inductors are neglected in the following analytical calculations. The resulting arm voltages may contain a zero-sequence $v_0(t)$ and are:

$$\begin{aligned} v_{\mathrm{arm,a}}(t) &= -v_{\mathrm{grid,a}}(t) + v_0(t) = -V_{\mathrm{grid}} \cos(\omega t) + v_0(t) \\ v_{\mathrm{arm,b}}(t) &= -v_{\mathrm{grid,b}}(t) + v_0(t) = -V_{\mathrm{grid}} \cos(\omega t - 2\pi/3) + v_0(t) \\ v_{\mathrm{arm,c}}(t) &= -v_{\mathrm{grid,c}}(t) + v_0(t) = -V_{\mathrm{grid}} \cos(\omega t + 2\pi/3) + v_0(t) \end{aligned} \tag{3}$$

The resulting input arm powers are the product of the arm currents and voltages:

$$\begin{aligned} p_{\mathrm{arm,a}}(t) &= v_{\mathrm{arm,a}}(t) i_{\mathrm{arm,a}}(t) = V_{\mathrm{grid}} I_{\mathrm{grid}} \cos^2(\omega t) - v_0(t) I_{\mathrm{grid}} \cos(\omega t) \\ p_{\mathrm{arm,b}}(t) &= v_{\mathrm{arm,b}}(t) i_{\mathrm{arm,b}}(t) = V_{\mathrm{grid}} I_{\mathrm{grid}} \cos^2(\omega t - 2\pi/3) - v_0(t) I_{\mathrm{grid}} \cos(\omega t - 2\pi/3) \\ p_{\mathrm{arm,c}}(t) &= v_{\mathrm{arm,c}}(t) i_{\mathrm{arm,c}}(t) = V_{\mathrm{grid}} I_{\mathrm{grid}} \cos^2(\omega t + 2\pi/3) - v_0(t) I_{\mathrm{grid}} \cos(\omega t + 2\pi/3) \end{aligned} \tag{4}$$

It should be noted, that $v_0(t)$ is the zero-sequence voltage, i.e. the voltage difference of the star point to the grid neutral N. It is often used to achieve power balance for an unbalanced grid or faulty modules [28–31]. The resulting arm voltages and input arm powers are shown in Fig. 3 for the nominal operation of $v_0(t) = 0$. In order to achieve steady-state, the isolated DC-DC converters in each arm have to transfer the average power of $P_{\mathrm{arm,avg}} = \frac{1}{T} \int_0^T V_{\mathrm{grid}} I_{\mathrm{grid}} \cos^2(\frac{2\pi}{T} t) dt = \frac{1}{2} V_{\mathrm{grid}} I_{\mathrm{grid}}$ to the load. However, the input arm power is not constant, which results in a second harmonic voltage ripple of the DC-link voltages.

Now, the net input power of the DC-link capacitors in arm 'a' is calculated for nominal operation and it is identical for the other two arms:

$$\begin{aligned} p_{\mathrm{DC,Link,Nominal,a}}(t) &= v_{\mathrm{arm,a}}(t) i_{\mathrm{arm,a}}(t) - P_{\mathrm{arm,avg}} = V_{\mathrm{grid}} I_{\mathrm{grid}} \cos^2(\omega t) - \tfrac{1}{2} V_{\mathrm{grid}} I_{\mathrm{grid}} \\ &= \tfrac{1}{2} V_{\mathrm{grid}} I_{\mathrm{grid}} \cos(2\omega t) = P_{\mathrm{arm,avg}} \cos(2\omega t) \end{aligned} \tag{5}$$

Between $t_1 = \frac{3}{8}\,\mathrm{T} = \frac{3}{8} \cdot \frac{2\pi}{\omega}$ and $t_2 = \frac{5}{8}\,\mathrm{T} = \frac{5}{8} \cdot \frac{2\pi}{\omega}$, the input power $p_{\mathrm{DC,Link,Nominal,a}}(t)$ of the DC-link capacitors in arm 'a' is positive, which causes the second harmonic voltage ripple. The energy, which has to be stored in the DC-link capacitors is highlighted in green in Fig. 3 and can be calculated as:

$$\Delta E_{\mathrm{Ripple,Nominal,a}} = \int_{t_1}^{t_2} p_{\mathrm{DC,Link,Nominal,a}}(t) dt = \int_{\frac{3}{8} \cdot \frac{2\pi}{\omega}}^{\frac{5}{8} \cdot \frac{2\pi}{\omega}} P_{\mathrm{arm,avg}} \cos(2\omega t) dt = P_{\mathrm{arm,avg}} \cdot \frac{1}{\omega} \tag{6}$$

For a transferred power of $P_{\mathrm{arm,avg}} = 1\,\mathrm{MW}$ per arm and a grid frequency of $50\,\mathrm{Hz}$, the DC-link capacitors have to buffer the energy of $\Delta E_{\mathrm{Ripple,Nominal,a}} = 3.2\,\mathrm{kJ}$ for each arm.

III. Third-Harmonic Zero-Sequence Voltage Injection

As shown in the previous Section II, the nominal stored energy in the DC-link capacitors is significant and increases the costs and volume of the overall system. Consequently, a commonly utilized technique is a third-harmonic voltage injection with $\frac{1}{6}$ of the grid voltage amplitude [32–35]. The resulting zero-sequence voltage injection can be expressed as:

$$v_{0,\mathrm{3rd}}(t) = \frac{1}{6} V_{\mathrm{grid}} \cos(3\omega t) \tag{7}$$

The arm voltages and input arm powers are calculated with Eq. (3) and Eq. (4) respectively and are shown in Fig. 4.

They show two major advantages compared to no voltage injection shown in Fig. 3. Firstly, the required arm voltages are reduced to $\frac{\sqrt{3}}{2} V_{\mathrm{grid}}$, which allows to reduce the number of modules in each arm by around $13.4\,\%$. Secondly, the peak input power of each arm is reduced by $\frac{1}{6}$, which reduces the enclosed area between an arm's input power and the DC-DC converter power $P_{\mathrm{arm,avg}}$ by $15.1\,\%$.
Now, these advantages of the third-harmonic injection are analytically derived with the same procedure as for the case with no injection. Again, only arm 'a' is considered and modulation artifacts shall be out of

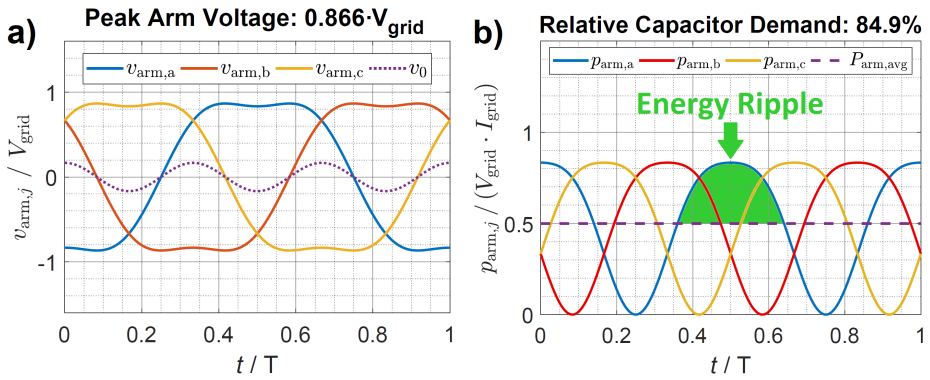

Fig. 4: Resulting arm voltages a) and input power b) for the third harmonic zero-sequence voltage injection. The required arm voltage is reduced to $\frac{\sqrt{3}}{2} V_{\text{grid}} = 0.866 V_{\text{grid}}$ and the energy ripple to 84.9 %.

the scope of this analysis. The net input power of the DC-link capacitors in arm 'a' can be expressed as:

$$\begin{aligned} & p_{\text{DC,Link,3rd,a}}(t) = v_{\text{arm,a}}(t) i_{\text{arm,a}}(t) - P_{\text{arm,avg}} \\ & = V_{\text{grid}} I_{\text{grid}} \cos^2(\omega t) - v_{0,\text{3rd}}(t) I_{\text{grid}} \cos(\omega t) - P_{\text{arm,avg}} \\ & = V_{\text{grid}} I_{\text{grid}} \cos^2(\omega t) - \tfrac{1}{6} V_{\text{grid}} I_{\text{grid}} \cos(3\omega t) \cos(\omega t) - P_{\text{arm,avg}} \\ & = 2 P_{\text{arm,avg}} \cos^2(\omega t) - \tfrac{1}{3} P_{\text{arm,avg}} \cos(3\omega t) \cos(\omega t) - P_{\text{arm,avg}} \\ & = \tfrac{1}{6} P_{\text{arm,avg}} (5\cos(2\omega t) - \cos(4\omega t)) \end{aligned} \tag{8}$$

The power $p_{\text{DC,Link,3rd,a}}(t)$ is positive between $t_{1,\text{3rd}} = 0.3601 \cdot \text{T} = 0.3601 \cdot \frac{2\pi}{\omega}$ and $t_{2,\text{3rd}} = 0.6399 \cdot \text{T} = 0.6399 \cdot \frac{2\pi}{\omega}$ (numerically calculated), which is only a slight deviation compared to the nominal operation. Consequently, the DC-link capacitors in arm 'a' have to buffer the energy of:

$$\begin{aligned} & \Delta E_{\text{Ripple,3rd,a}} = \int_{t_{1,\text{3rd}}}^{t_{2,\text{3rd}}} p_{\text{DC,Link,3rd,a}}(t) dt \\ & = \int_{0.3601 \cdot \frac{2\pi}{\omega}}^{0.6399 \cdot \frac{2\pi}{\omega}} \tfrac{1}{6} P_{\text{arm,avg}} (5\cos(2\omega t) - \cos(4\omega t)) dt = P_{\text{arm,avg}} \cdot \tfrac{1}{\omega} \cdot \mathbf{0.849} \\ & = \Delta E_{\text{Ripple,Nominal,a}} \cdot \mathbf{0.849} \end{aligned} \tag{9}$$

IV. Min-Max Zero-Sequence Voltage Injection

Another commonly used technique is the Min-Max zero-sequence voltage injection and it shares many similarities with the third-harmonic injection shown in Section III. The offset voltage $v_0(t)$ is calculated with a well-known equation to minimize the instantaneous value of arm voltages [36–38]:

$$v_{0,\text{MinMax}}(t) = \frac{\max(v_{\text{grid,a}}(t), v_{\text{grid,b}}(t), v_{\text{grid,c}}(t)) + \min(v_{\text{grid,a}}(t), v_{\text{grid,b}}(t), v_{\text{grid,c}}(t))}{2} \tag{10}$$

The resulting Min-Max voltage injection is shown in Fig. 5. Exactly like by the 3rd harmonic injection, the peak arm voltage is reduced by 13.4% (to $\frac{\sqrt{3}}{2}$). However, the Min-Max injection has a benefit regarding the second harmonic voltage ripple. Now the DC-link capacitors in arm 'a' have to buffer the energy:

$$\Delta E_{\text{Ripple,MinMax,a}} = 0.812\, \Delta E_{\text{Ripple,Nominal,a}} = 0.956 \Delta E_{\text{Ripple,3rd,a}} \tag{11}$$

In Fig. 6 the three discussed voltage injection techniques are shown for one arm to explain why the Min-Max voltage injection performs better than the 3rd harmonic injection. For $t = 0.5\,\text{T}$, the arm current $i_{\text{arm,a}}(t)$ reaches its peak value as shown in Fig. 2b). Without a zero-sequence injection the arm voltage $v_{\text{arm,a}}(t)$ also reaches its peak value for $t = 0.5\,\text{T}$. This has the consequence, that for $t = 0.5\,\text{T}$ the module capacitors in arm 'a' receive $2/3$ of the total input power while accounting for only $1/3$ of all modules.

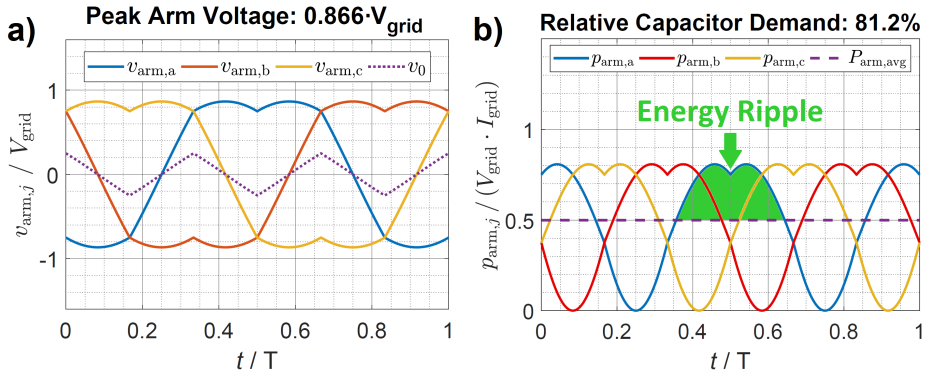

Fig. 5: Resulting arm voltages a) and input power b) for the Min-Max zero-sequence voltage injection. It requires a 4.4 % smaller DC-link capacitance $C_{\mathrm{DC,Link}}$ compared to the third-harmonic injection.

With the Min-Max zero-sequence voltage injection, the arm voltage of arm 'a' is reduced by $1/4$ compared to the nominal case for $t = 0.5\,\mathrm{T}$. As the input arm power is the product of the arm voltage and the (still same) arm current, the reduction of the input power of arm 'a' at $t = 0.5\,\mathrm{T}$ is clearly visible. As a result, the enclosed area between p_{MinMax} and $P_{\mathrm{arm,avg}}$ is reduced by 4.4 % compared to the third-harmonic voltage injection p_{3rd} and even by 18.8 % compared to no zero-sequence voltage injection p_{Nom}.

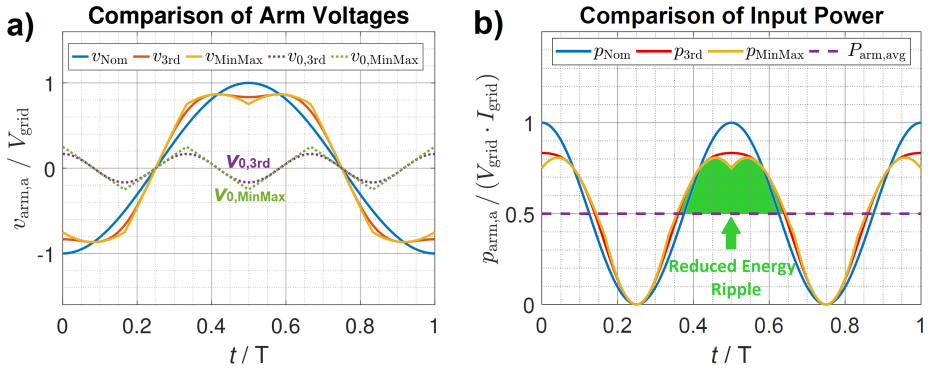

Fig. 6: Comparison of 3rd-harmonic voltage injection to Min-Max and no voltage injection for arm 'a'.

V. Novel Saturation Zero-Sequence Voltage Injection

The third-harmonic and especially the Min-Max zero-sequence voltage injections show a significant reduction of the energy which has to be buffered by the DC-link capacitors $C_{\mathrm{DC,Link}}$ in each fundamental cycle. The zero-sequence voltage injection $v_0(t)$ can be selected freely as long as the resulting arm voltages are not larger than the maximum possible arm voltages $\hat{v}_{\mathrm{arm},j}(t) = v_{\mathrm{DC},jn}(t) \cdot N_{\mathrm{arm},j}$ for $j = \{\mathrm{a},\mathrm{b},\mathrm{c}\}$. The maximum possible arm voltage $\hat{v}_{\mathrm{arm},j}(t)$ of each arm depends on the nominal DC-link voltage and the number of modules connected in series. One of the three arms is operating at its positive voltage limit, if the voltage injection of $v_{0,\mathrm{Max}}(t)$ is selected [31]:

$$v_{0,\mathrm{Max}}(t) = \min(\hat{v}_{\mathrm{arm,a}}(t) + v_{\mathrm{grid,a}}(t), \hat{v}_{\mathrm{arm,b}}(t) + v_{\mathrm{grid,b}}(t), \hat{v}_{\mathrm{arm,c}}(t) + v_{\mathrm{grid,c}}(t)) \tag{12}$$

The following voltage injection allows to operate one arm at its negative voltage limit:

$$v_{0,\mathrm{Min}}(t) = -\min(\hat{v}_{\mathrm{arm,a}}(t) - v_{\mathrm{grid,a}}(t), \hat{v}_{\mathrm{arm,b}}(t) - v_{\mathrm{grid,b}}(t), \hat{v}_{\mathrm{arm,c}}(t) - v_{\mathrm{grid,c}}(t)) \tag{13}$$

In practice, the controller must account for the instantaneous voltage ripple, so the maximum available arm voltage $\hat{v}_{\mathrm{arm},j}(t)$ for each arm $j = \{\mathrm{a},\mathrm{b},\mathrm{c}\}$ is time, load and capacitor size dependent. For analytical purposes, these factors are neglected and constant maximum available arm voltages $\hat{v}_{\mathrm{arm,a}}(t) = \hat{v}_{\mathrm{arm,b}}(t) =$

$\hat{v}_{\mathrm{arm,c}}(t) = \hat{v}_{\mathrm{arm},j}$ are assumed. Eq. (12) and Eq. (13) are simplified to:

$$\begin{aligned} v_{0,\mathrm{Max}}(t) &= \hat{v}_{\mathrm{arm},j} + \min(v_{\mathrm{grid,a}}(t), v_{\mathrm{grid,b}}(t), v_{\mathrm{grid,c}}(t)) \\ v_{0,\mathrm{Min}}(t) &= -\hat{v}_{\mathrm{arm},j} - \min(-v_{\mathrm{grid,a}}(t), -v_{\mathrm{grid,b}}(t), -v_{\mathrm{grid,c}}(t)) \end{aligned} \tag{14}$$

Any selected voltage injection must fulfill the condition $v_{0,\mathrm{Min}}(t) \leq v_0(t) \leq v_{0,\mathrm{Max}}(t)$. A third harmonic zero-sequence voltage injection with the grid voltage amplitude halves the DC-link capacitor demand [34], but requires over 77 % additional modules per arm compared to the Min-Max injection. Therefore, the new proposed method uses the third-harmonic injection to calculate the offset voltage. In case, that the offset voltage violates the criterion $v_{0,\mathrm{Min}}(t) \leq v_0(t) \leq v_{0,\mathrm{Max}}(t)$, it is set to $v_{0,\mathrm{Min}}(t)$ or $v_{0,\mathrm{Max}}(t)$:

$$v_{0,\mathrm{Saturation}}(t) = \max(\min(V_{\mathrm{grid}} \cos(3\omega t), v_{0,\mathrm{Max}}(t)), v_{0,\mathrm{Min}}(t)) \tag{15}$$

The resulting arm voltages for the proposed method are plot in Fig. 7. The arm voltage limit of $\hat{v}_{\mathrm{arm},j} = \frac{\sqrt{3}}{2} V_{\mathrm{grid}}$ is selected to have the same peak arm voltages as the Min-Max injection. It extends the advantage of the Min-Max Injection by further reducing the arm voltage at the time instant of maximum arm current. The resulting energy ripple is numerically calculated and finally decreased to 75.7 %. This means, that the new method requires less than 24 % DC-link capacitance when compared to the standard method.
In order to verify, that the trajectory of the zero-sequence is optimal, a genetic algorithm similar to [39] is implemented. It approximates the shape of the zero-sequence with $v_{0,\mathrm{Genetic}}(t) = \hat{v}_{0,3} \cos(3\omega t) + \hat{v}_{0,9} \cos(9\omega t) + \hat{v}_{0,15} \cos(15\omega t)$ and optimizes to coefficients $\hat{v}_{0,3}$, $\hat{v}_{0,9}$ and $\hat{v}_{0,15}$ to minimize the energy ripple and ensure $\hat{v}_{\mathrm{arm},j} = \frac{\sqrt{3}}{2} V_{\mathrm{grid}}$. The resulting arm voltages shown in Fig. 7c) are indeed very similar to Fig. 7a) and show no advantage in respect to the energy ripple reduction. The optimal coefficients depend on the available arm voltage, as it can be seen in Fig. 8c). Again, the optimal zero-sequence calculated by the genetic algorithm is achieved with the much simpler proposed equation Eq. (15).

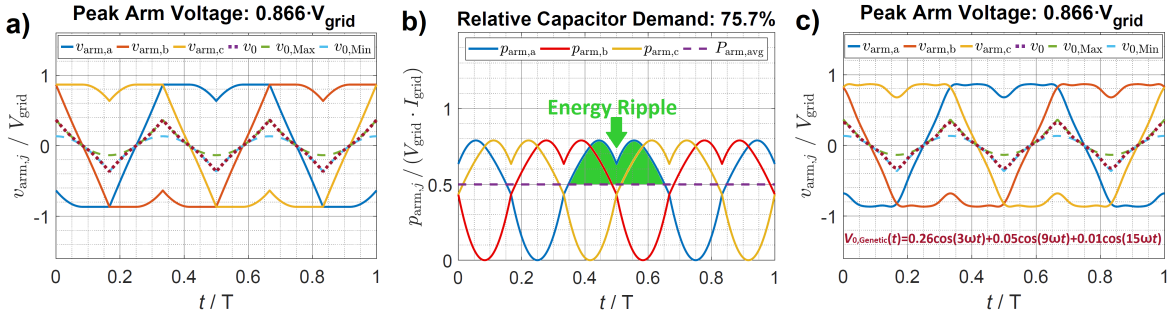

Fig. 7: Resulting arm voltages a) and input power b) for the proposed saturation zero-sequence voltage injection. The required arm voltage is reduced to $\frac{\sqrt{3}}{2} V_{\mathrm{grid}} = 0.866 V_{\mathrm{grid}}$ and the energy ripple to 75.7 %.

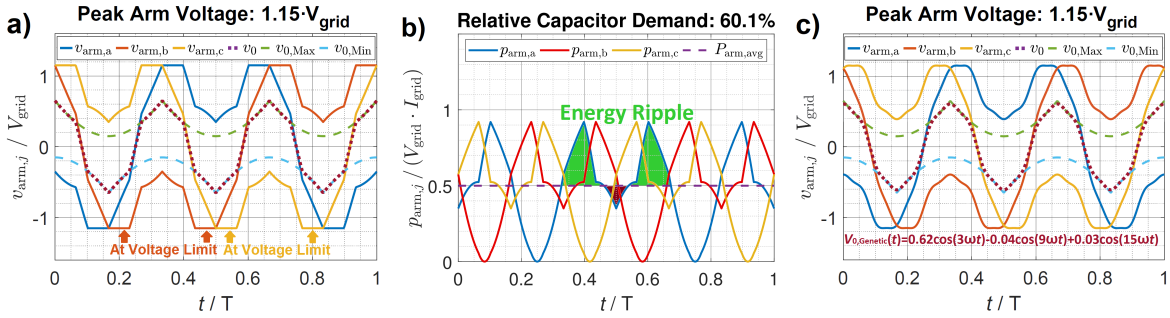

Fig. 8: Resulting arm voltages and input power for the proposed saturation zero-sequence voltage injection. An available arm voltage of $1.15 V_{\mathrm{grid}}$ reduces the energy ripple to 60.1 %. So, $C_{\mathrm{DC,Link}}$ can be reduced by 40 %.

Usually, the arm voltage is not strictly limited to $\frac{\sqrt{3}}{2} V_{\text{grid}}$ because several reserve modules are available to compensate faulty modules and grid-side overvoltages. Additionally, the cell voltages of the PEM electrolyzers can reach 2.2 V at full load at 3 $\frac{\text{A}}{\text{cm}^2}$ due to the ohmic resistance of the cell membrane, gas pressure, water temperature as well as other factors [2], while it is only 1.4 V at light load. In large-scale electrolyzers, several hundred cells are connected in series, but the resulting load voltage v_{DC} still has the same relative variation as a single cell.

In order to operate the isolated DC-DC converter (LLC resonant converter) at or at least close to the efficient resonance condition [20] at light load, the DC-link voltage of each module has to be lower than at full load. This additional available arm voltage (at full load) can be used to decrease the second harmonic voltage ripple. The resulting arm voltages of the proposed method are shown in Fig. 8a), if the peak available arm voltage is 15 % higher than the peak grid voltage. This results in a further decrease of the second harmonic voltage ripple and therefore of the capacitor size requirement. It should be noted, that usually one arm is operating at its positive or negative voltage limit. This is the case, if the offset voltage $v_{0,\text{Saturation}}(t)$ is set to $v_{0,\text{Max}}(t)$ or $v_{0,\text{Min}}(t)$. As a positive side effect, this also reduces the number of switching actions in the AC-DC stage by nearly 33 % because usually one arm is clamped.

The following table summarizes the required arm voltages and resulting energy ripples for standard methods as well as the newly proposed method. The proposed saturation injection outperforms the commonly used 3rd harmonic and Min-Max injection methods even if only a small arm voltage of $\frac{\sqrt{3}}{2} V_{\text{grid}} = 0.866 V_{\text{grid}}$ is available. In addition, the energy ripple decreases, if more reserve modules are available. For unrealistically high available arm voltages of 54 % above grid voltage ($\hat{v}_{\text{arm},j} \geq \frac{16}{9} \frac{\sqrt{3}}{2} V_{\text{grid}} = 1.54 V_{\text{grid}}$), the proposed voltage injection is equivalent to $v_{0,\text{Saturation}}(t) = V_{\text{grid}} \cos(3\omega t)$. The 2nd harmonic voltage ripple is converted to a 4th harmonic voltage ripple, which has twice the frequency and therefore half the energy ripple.

Zero-Sequence Voltage Injection	Normalized Peak Arm Voltage	Normalized Energy Ripple
Nominal	1.000	1.000
3rd Harmonic	0.866	0.849
Min-Max	0.866	0.812
Saturation (Proposed)	0.866	0.757
Saturation (Proposed)	1.15	0.601
Saturation (Proposed)	1.54	0.500

Tab. 1: Required arm voltage and resulting energy ripple for investigated methods. The proposed saturation modulation performs best and requires the least amount of DC-link capacitance.

VI. Conclusion

A new saturation-based zero-sequence voltage injection for modular cascaded H-bridge (CHB) with star configuration has been proposed and analytically verified. First, the commonly used techniques of the 3rd harmonic and Min-Max zero-sequence voltage injection were evaluated. As a result, the Min-Max injection reduces the second harmonic voltage ripple by 18.8 % while the third-harmonic injection with $\frac{1}{6}$ of the grid voltage amplitude reduces the voltage ripple by only 15.1 %. This is achieved by distributing the input power more evenly across the three arm capacitors by preventing too high instantaneous arm voltages in combination with high arm currents.

The proposed zero-sequence injection technique usually operates the arm with the second largest absolute current at its voltage limit to minimize the arm voltage of the arm with the maximum current. This has the advance of reducing the energy to be buffered by the module DC-link capacitors between 24.3 % and 40 % depending on the available arm voltage. Commonly, several reserve modules are available to compensate for grid-overvoltages and modules faults. However, most of the time this is not required and a large arm voltage reserve is available, which is utilized by the proposed voltage injection technique. Finally, the costs and volume of the DC-link capacitors are reduced by 40 % compared to the nominal operation of CHBs operating as AC-DC converters for large-scale water electrolyzers.

References

[1] M. Kuprat, M. Bending, and K. Pfeiffer. “Possible role of power-to-heat and power-to-gas as flexible loads in German medium voltage networks”. In: *Frontiers in Energy* 11 (2017), pp. 135–145.

[2] Geert Hauke Tjarks. “PEM-Electrolysis-Systems for the Integration in Power-to-Gas Applications”. In: *Doctoral dissertation, Ph. D. thesis, RWTH Aachen University* (2017).

[3] Thomas Grube, Larissa Doré, André Hoffrichter, Laura Elisabeth Hombach, Stephan Raths, et al. “An option for stranded renewables: electrolytic-hydrogen in future energy systems”. In: *Sustainable Energy Fuels* 2 (2018), pp. 1500–1515.

[4] J. Solanki. “High Power Factor High-Current Variable-Voltage Rectifiers”. In: *Dissertation, Paderborn University, Germany* (2015).

[5] Mengxing Chen, Shih-Feng Chou, Frede Blaabjerg, and Pooya Davari. “Overview of Power Electronic Converter Topologies Enabling Large-Scale Hydrogen Production via Water Electrolysis”. In: *Applied Sciences* 12.4 (2022).

[6] A. Pratt, P. Kumar, and T. V. Aldridge. “Evaluation of 400V DC Distribution in Telco and Data Centers to Improve Energy Efficiency”. In: *INTELEC 07 - 29th Int. Telecommunications Energy Conf.* 2007, pp. 32–39.

[7] Jonas Huber, Peter Wallmeier, Ralf Pieper, Frank Schafmeister, and Johann W Kolar. “Comparative Evaluation of MVAC-LVDC SST and Hybrid Transformer Concepts for Future Datacenters”. In: (2022).

[8] Hao Tu, Hao Feng, Srdjan Srdic, and Srdjan Lukic. “Extreme Fast Charging of Electric Vehicles: A Technology Overview”. In: *IEEE Transactions on Transportation Electrification* 5.4 (2019), pp. 861–878.

[9] Burin Yodwong, Damien Guilbert, Matheepot Phattanasak, Wattana Kaewmanee, Melika Hinaje, and Gianpaolo Vitale. “AC-DC Converters for Electrolyzer Applications: State of the Art and Future Challenges”. In: *Electronics* 9.6 (2020).

[10] J. R. Rodriguez, J. Pontt, C. Silva, E. P. Wiechmann, P. W. Hammond, et al. “Large current rectifiers: State of the art and future trends”. In: *IEEE Transactions on Industrial Electronics* 52.3 (2005), pp. 738–746.

[11] Joonas Koponen, Vesa Ruuskanen, Antti Kosonen, Markku Niemelä, and Jero Ahola. “Effect of Converter Topology on the Specific Energy Consumption of Alkaline Water Electrolyzers”. In: *IEEE Transactions on Power Electronics* 34.7 (2019), pp. 6171–6182.

[12] Vesa Ruuskanen, Joonas Koponen, Antti Kosonen, Markku Niemelä, Jero Ahola, and Aki Hämäläinen. “Power quality and reactive power of water electrolyzers supplied with thyristor converters”. In: *Journal of Power Sources* 459 (2020).

[13] Sanzhong Bai and Srdjan M. Lukic. “New Method to Achieve AC Harmonic Elimination and Energy Storage Integration for 12-Pulse Diode Rectifiers”. In: *IEEE Transactions on Industrial Electronics* 60.7 (2013), pp. 2547–2554.

[14] K. D. McBee and M. G. Simões. “Evaluating the Long-Term Impact of a Continuously Increasing Harmonic Demand on Feeder-Level Voltage Distortion”. In: *IEEE Trans. Ind. App.* 50.3 (2014), pp. 2142–2149.

[15] H. Akagi, S. Inoue, and T. Yoshii. “Control and Performance of a Transformerless Cascade PWM STATCOM With Star Configuration”. In: *IEEE Transactions on Industry Applications* 43.4 (2007), pp. 1041–1049.

[16] Q. Song and W. Liu. “Control of a Cascade STATCOM With Star Configuration Under Unbalanced Conditions”. In: *IEEE Transactions on Power Electronics* 24.1 (2009), pp. 45–58.

[17] T. Tanaka, K. Ma, H. Wang, and F. Blaabjerg. “Asymmetrical Reactive Power Capability of Modular Multilevel Cascade Converter Based STATCOMs for Offshore Wind Farm”. In: *IEEE Transactions on Power Electronics* 34.6 (2019), pp. 5147–5164.

[18] J. Solanki, N. Fröhleke, J. Böcker, and P. Wallmeier. “A modular multilevel converter based high-power high-current power supply”. In: *IEEE Int. Conference on Industrial Technology (ICIT)*. 2013, pp. 444–450.

[19] Roland Unruh, Frank Schafmeister, and Joachim Böcker. “Evaluation of MMCs for High-Power Low-Voltage DC-Applications in Combination with the Module LLC-Design”. In: *2020 22nd European Conference on Power Electronics and Applications (EPE’20 ECCE Europe)*. 2020.

[20] Roland Unruh, Frank Schafmeister, and Joachim Böcker. “11kW, 70kHz LLC Converter Design with Adaptive Input Voltage for 98% Efficiency in an MMC”. In: *2020 IEEE 21st Workshop on Control and Modeling for Power Electronics (COMPEL)*. 2020, pp. 1–8.

[21] J. Kim, C. Kim, J. Kim, J. Lee, and G. Moon. “Analysis on Load-Adaptive Phase-Shift Control for High Efficiency Full-Bridge LLC Resonant Converter Under Light-Load Conditions”. In: *IEEE Transactions on Power Electronics* 31 (2016), pp. 4942–4955.

[22] P. Rehlaender, R. Unruh, F. Schafmeister, and J. Böcker. “Alternating Asymmetrical Phase-Shift Modulation for Full-Bridge Converters with Balanced Switching Losses to Reduce Thermal Imbalances”. In: *IEEE Applied Power Electronics Conference and Exposition (APEC)*. 2021.

[23] J. E. Huber and J. W. Kolar. “Volume/weight/cost comparison of a 1MVA 10 kV/400 V solid-state against a conventional low-frequency distribution transformer”. In: *ECCE*. 2014, pp. 4545–4552.

[24] Zheqing Li, Yi-Hsun Hsieh, Qiang Li, Fred C. Lee, and Chunyang Zhao. “Evaluation of Double-Line-Frequency Power Flow in Solid-State Transformers”. In: *2021 IEEE Fourth International Conference on DC Microgrids (ICDCM)*. 2021.

[25] T. Zhao, G. Wang, S. Bhattacharya, and A. Q. Huang. “Voltage and Power Balance Control for a Cascaded H-Bridge Converter-Based Solid-State Transformer”. In: *IEEE Transactions on Power Electronics* 28.4 (2013), pp. 1523–1532.

[26] H. Bärnklau, A. Gensior, and S. Bernet. “Derivation of an equivalent submodule per arm for modular multilevel converters”. In: *15th Int. Power Electronics and Motion Control Conf. (EPE/PEMC)*. 2012.

[27] Youngjong Ko, Anatolii Tcai, and Marco Liserre. “DC-Link Voltage Balancing Modulation for Cascaded H-Bridge Converters”. In: *IEEE Access* 9 (2021), pp. 103524–103532.

[28] L. Wang, D. Zhang, Y. Wang, B. Wu, and H. S. Athab. “Power and Voltage Balance Control of a Novel Three-Phase Solid-State Transformer Using Multilevel Cascaded H-Bridge Inverters for Microgrid Applications”. In: *IEEE Transactions on Power Electronics* 31.4 (2016), pp. 3289–3301.

[29] F. V. Amaral, T. M. Parreiras, G. C. Lobato, A. A. P. Machado, I. A. Pires, and B. de Jesus Cardoso Filho. “Operation of a Grid-Tied Cascaded Multilevel Converter Based on a Forward Solid-State Transformer Under Unbalanced PV Power Generation”. In: *IEEE Trans. on Industry App.* 54.5 (2018), pp. 5493–5503.

[30] T. Zhao, X. Zhang, M. Wang, W. Mao, F. Li, et al. “Module Power Balance Control and Redundancy Design Analysis of Cascaded PV Solid State Transformer under Fault Conditions”. In: *IEEE Journal of Emerging and Selected Topics in Power Electronics* (2020).

[31] R. Unruh, J. Lange, F. Schafmeister, and J. Böcker. “Adaptive Zero-Sequence Voltage Injection for Modular Solid-State Transformer to Compensate for Asymmetrical Fault Conditions”. In: *2021 23rd European Conference on Power Electronics and Applications (EPE’21 ECCE Europe)*. 2021.

[32] Yifan Yu, Georgios Konstantinou, Branislav Hredzak, and Vassilios G. Agelidis. “On extending the energy balancing limit of multilevel cascaded H-bridge converters for large-scale photovoltaic farms”. In: *2013 Australasian Universities Power Engineering Conference (AUPEC)*. 2013, pp. 1–6.

[33] Y. Yu, G. Konstantinou, B. Hredzak, and V. G. Agelidis. “Power Balance of Cascaded H-Bridge Multilevel Converters for Large-Scale Photovoltaic Integration”. In: *IEEE Transactions on Power Electronics* 31.1 (2016), pp. 292–303.

[34] Y. Hu, X. Zhang, W. Mao, T. Zhao, F. Wang, and Z. Dai. “An Optimized Third Harmonic Injection Method for Reducing DC-Link Voltage Fluctuation and Alleviating Power Imbalance of Three-Phase Cascaded H-Bridge Photovoltaic Inverter”. In: *IEEE Trans. on Industrial Electronics* 67.4 (2020), pp. 2488–2498.

[35] Y. Hu, Z. Li, H. Zhang, C. Zhao, F. Gao, et al. “High-Frequency-Link Current Stress Optimization of Cascaded H-Bridge-Based Solid-State Transformer With Third-Order Harmonic Voltage Injection”. In: *IEEE Journal of Emerging and Selected Topics in Power Electronics* 9.1 (2021), pp. 1027–1038.

[36] S. Rivera, B. Wu, S. Kouro, H. Wang, and D. Zhang. “Cascaded H-bridge multilevel converter topology and three-phase balance control for large scale photovoltaic systems”. In: *2012 3rd IEEE International Symposium on Power Electronics for Distributed Generation Systems (PEDG)*. 2012, pp. 690–697.

[37] B. P. McGrath, D. G. Holmes, and T. Lipo. “Optimized space vector switching sequences for multilevel inverters”. In: *IEEE Transactions on Power Electronics* 18.6 (2003), pp. 1293–1301.

[38] S. Haghbin and T. Thiringer. “DC bus current harmonics of a three-phase PWM inverter with the zero sequence injection”. In: *2014 IEEE Transportation Electrification Conf. and Expo (ITEC)*. 2014, pp. 1–6.

[39] Simon Fuchs, Min Jeong, and Jürgen Biela. “Reducing the Energy Storage Requirements of Modular Multilevel Converters with Optimal Capacitor Voltage Trajectory Shaping”. In: *2020 22nd European Conference on Power Electronics and Applications (EPE’20 ECCE Europe)*. 2020.